Journal of Molecular Catalysis A: Chemical 374–375 (2013) 111–117

Contents lists available at SciVerse ScienceDirect

Journal of Molecular Catalysis A: Chemical

journal homepage: www.elsevier.com/locate/molcata

Enhancing the photocatalytic activity of lead molybdate by modifying with fullerene

Ke Dai [a], Yong Yao [b], Hui Liu [b], Ibrahim Mohamed [c], Hao Chen [b,*], Qiaoyun Huang [a]

[a] College of Resources and Environment, Huazhong Agricultural University, Wuhan 430070, PR China
[b] College of Science, Huazhong Agricultural University, Wuhan 430070, PR China
[c] Faculty of Agriculture, Benha University, Moshtohor, 13736 Qalubia, Egypt

ARTICLE INFO

Article history:
Received 19 January 2013
Received in revised form 24 March 2013
Accepted 25 March 2013
Available online 10 April 2013

Keywords:
Fullerenes
Semiconductors
Lead molybdate
Nanocomposites
Photocatalytic degradation

ABSTRACT

In this study, fullerene-modified lead molybdate (C_{60}–$PbMoO_4$) was prepared via a hydrothermal method, and characterized by X-ray diffraction, UV–vis diffuse reflection spectroscopy, high-resolution transmission electron microscopy, Raman spectroscopy, and X-ray photoelectron spectroscopy. It was shown that the introduction of C_{60} reduces the crystallite size of $PbMoO_4$, slightly influences the textual properties and optical characteristics (UV–vis absorption). The effect of C_{60} content on the photocatalytic activity of C_{60}–$PbMoO_4$ was studied in the photocatalytic degradation of rhodamine B under UV light and visible light irradiation. After modification with C_{60}, the photocatalytic activity of $PbMoO_4$ increased 3.8 times at a C_{60} weight ratio of 0.5 wt% under UV light irradiation, and 4.1 times at a C_{60} weight ratio of 5.0 wt% under visible light irradiation. The significant photocatalytic activity of C_{60}–$PbMoO_4$ was attributed to the excellent light absorption and charge separation on the interfaces between C_{60} and $PbMoO_4$.

1. Introduction

Environmental pollution and destruction on a global scale are issues of increasing concern in today's society [1–4]. There is a need for effective method for removal of pollutants [5–10]. Photocatalysis has been widely used as a unique treatment for the destruction of organic pollutants [11–16]. Up till now, TiO_2 has been extensively investigated as the most important photocatalyst [17]. But the large band gap and quick recombination of charge carriers of TiO_2 limits its application [18,19]. Molybdates such as $Ag_2Mo_4O_{13}$, $CdMoO_4$, Bi_2MoO_6, $PbMoO_4$, and others have emerged as attractive alternatives to TiO_2 and have been widely studied in recent years [20–24]. However, few molybdates exhibit efficient photocatalytic activity under visible light irradiation. Several methods are employed to modify the molybdates and to enhance their photocatalytic activity, including controlling their morphology and exposed facets [25,26], doping with metals [27] or nonmetal elements [28], coupling with other semiconductors [29] and hybridization with carbonaceous materials [30].

Carbon-based-material modified semiconductors demonstrate advantages such as strong absorption of visible light and high photocatalytic activity [31–33]. Fullerenes have unique three-dimensional structures for its delocalized π electrons. As the most representative fullerene species, C_{60} has been widely used in many fields for its superior performances [34,35]. Modifying semiconductor photocatalysts through the utilization of the special electronic properties of C_{60} can arouse rapid photoinduced charge separation and reduce electron–hole recombination, thus enhancing the photocatalytic activity [36]. Zhao and co-workers [37] have reported Bi_2MoO_4 nanoparticles via hydrothermal method and modified by C_{60}. It is observed that the photocatalytic activity in the reduction of bromate ions was increased by the C_{60} modification. Fu and co-workers [38] dispersed C_{60} with monomolecular layer state on the surface of ZnO and gained C_{60}-hybridized ZnO, of which showed enhanced photocatalytic activity for the degradation of methylene blue. Moreover, the hybridization of C_{60} also improved the photostability of ZnO. Furthermore, C_{60} modified Bi_2WO_6 photocatalysts were prepared by a simple absorbing process by Zhu et al. [39]. Much higher efficiency was obtained in degradation of methylene blue and rhodamine B (RhB). However, part of the research only synthesized a hybrid by the simple adsorption of C_{60} on the other semiconductors in toluene suspension [38,39]. It is reported that intimate contact in the hybrid would benefit the quick transfer of photogenerated electrons during the photocatalysis [40], which suggest the hybrid with chemical bonding between the two components would have better photoactivity than that with only adsorption.

In this study, for the first time, C_{60} modified lead molybdate (C_{60}–$PbMoO_4$) was synthesized through the hydrothermal method. The photocatalytic activities of C_{60}–$PbMoO_4$ with various contents of C_{60} were tested under UV light and visible light irradiation.

* Corresponding author. Tel.: +86 27 8728 7046; fax: +86 27 8728 7369.
E-mail address: hchenhao@mail.hzau.edu.cn (H. Chen).

1381-1169/$ – see front matter © 2013 Elsevier B.V. All rights reserved.
http://dx.doi.org/10.1016/j.molcata.2013.03.027

2. Experimental

2.1. Preparation of C_{60}–$PbMoO_4$

A high-purity (99.9%) C_{60} sample was purchased from Nanjing XFNano Material Tech Co., Ltd. The sample was functionalized by refluxing and stirring vigorously in 10% (w/w) HNO_3 for 2 h. After the treatment, the sample was subjected to centrifugation, decantation, and dilution with 18 MΩ cm deionized water until the supernatant pH became neutral. Resultant sample was dried for 8 h at 80 °C. C_{60}–$PbMoO_4$ was prepared as follows: the starting materials of $Pb(NO_3)_2$ were dissolved in 1.0 mol L^{-1} HNO_3 and mixed with $Mo_7O_{24}{\cdot}6(NH_4){\cdot}4(H_2O)$ aqueous solution with the molar ratio of 7:1. An appropriate amount of functionalized C_{60} was added to the solution, which was then stirred vigorously for 30 min. The suspension was transferred into a 100 mL Teflon-lined stainless steel autoclave and heated at 160 °C for 24 h. The resultant solid was separated via centrifugation, washed with water and ethanol several times, and then dried overnight at 60 °C.

2.2. Characterization

X-ray diffraction patterns of C_{60}–$PbMoO_4$ were recorded at room temperature by a Bruker D8 Advance X-ray diffractometer. Raman spectra were obtained on a Renishaw RM1000 spectrometer. The diffuse reflectance absorption spectra of the samples were recorded on a Shimadzu UV-3100 spectrophotometer equipped with an integrated sphere attachment. High-resolution transmission electron microscopy images were obtained by using a JEM 2100F field emission transmission electron microscope. X-ray photoemission spectroscopy was carried out by a Kratos Analytical XSAM800 spectrometer. Brunauer–Emmett–Teller specific surface areas (S_{BET}) of the samples were measured by nitrogen adsorption–desorption in a Micromeritics ASAP 2020 apparatus.

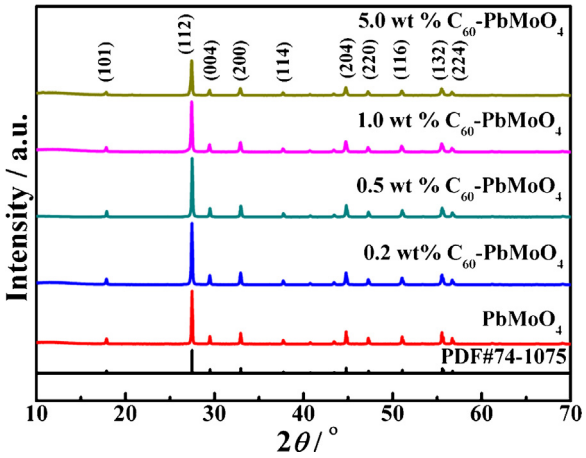

Fig. 1. XRD patterns of $PbMoO_4$ and C_{60}–$PbMoO_4$ with various contents of C_{60}.

2.3. Photocatalytic degradation

Photocatalytic degradation of dye can be used for testing the activity of photocatalyst [41,42]. The photocatalytic activities of C_{60}–$PbMoO_4$ were evaluated through the degradation of RhB under UV light and visible light irradiation. An 18 W low-pressure mercury lamp was used as the UV light source, with an average light intensity of 14.5 μW cm^{-2}. A 300 W Xenon lamp (PLS-SXE300C,

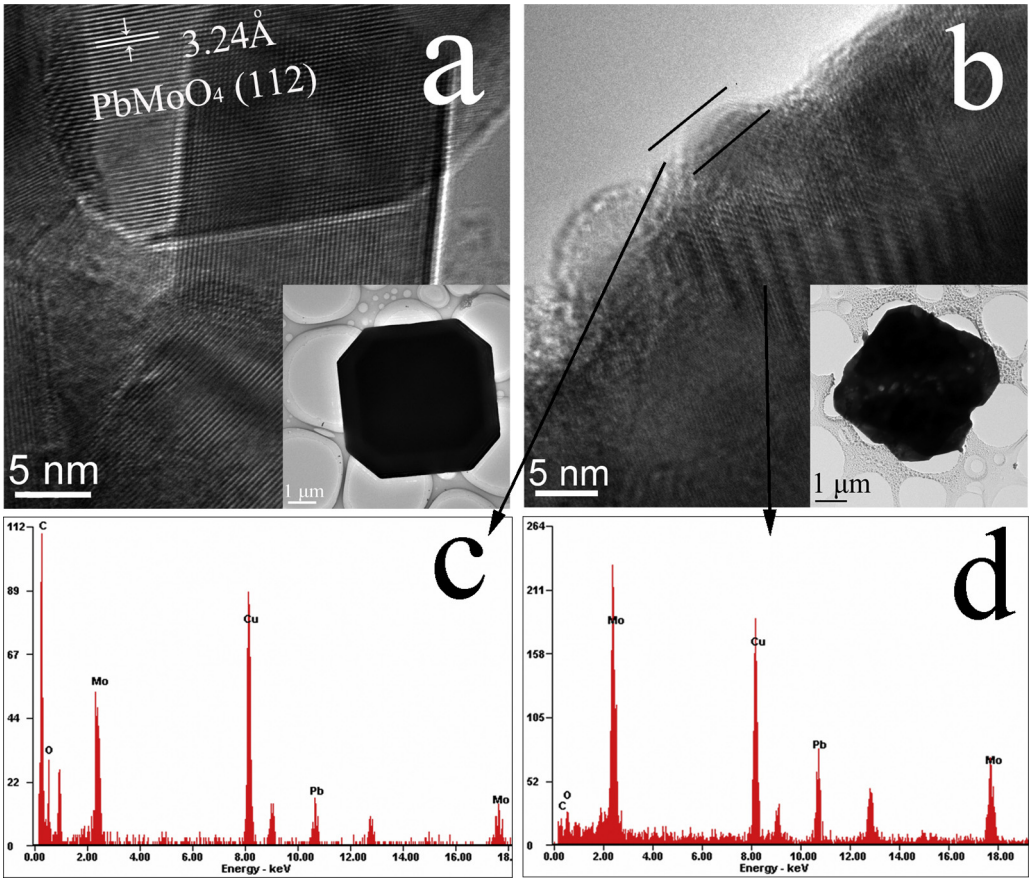

Fig. 2. HRTEM images of $PbMoO_4$ (a) and C_{60}–$PbMoO_4$ (b), EDS spectrum taken from the edge (c) and the center of C_{60}–$PbMoO_4$ sample (d).

Beijing) with a 420 nm cutoff filter was used as the visible light source, with an average light intensity of 600 μW cm^{-2}. In each experiment, 20 mg photocatalyst was added into 50 mL of RhB solution (1×10^{-5} M). Before irradiation, the suspensions were magnetically stirred in the dark for 30 min to achieve the adsorption equilibrium. Then the suspensions were exposed to UV light or visible light irradiation. At given irradiation time intervals, 3 mL of the suspension was collected and centrifuged to remove the photocatalyst. The centrifuged solution was analyzed by a Nicolet 300 evolution UV–vis spectrophotometer, monitoring the characteristic absorption peak of RhB at 554 nm to quantify the RhB concentration in the solution.

3. Results and discussion

3.1. Characterization of C_{60}–$PbMoO_4$

Fig. 1 illustrates the XRD patterns of C_{60}–$PbMoO_4$ with various contents of C_{60}. $PbMoO_4$ of pure phase is a tetragonal structure, and the corresponding JCPDS-ICDD number is 74-1075. The peaks at 27.5°, 32.9°, and 44.8° show an excellent match with the {1 1 2}, {2 0 0}, {1 1 4} crystal planes of wulfenite $PbMoO_4$. Comparing with that of $PbMoO_4$, the characteristic peaks of C_{60}–$PbMoO_4$ with various contents of C_{60} remain the same, indicating the lattice structure of $PbMoO_4$ did not changed after modification with C_{60}. However, the XRD patterns of C_{60}–$PbMoO_4$ with various contents of C_{60} showed different peak intensities.

As estimated according to the peak broadening based on the Scherrer equation, the mean crystallite sizes are 55.4, 50.2, 48.2, 43.3, and 40.8 nm for pure $PbMoO_4$ and C_{60}–$PbMoO_4$ with C_{60} contents of 0.2, 0.5, 1.0, and 5.0 wt%, respectively. The crystallite size clearly decreases gradually with the increase in C_{60} content, which demonstrates that the introduction of C_{60} can inhibits the growth of the $PbMoO_4$ grain and decrease the crystallinity of $PbMoO_4$.

As shown in Fig. 2a, one individual polyhedron can be observed as having a well-defined 18-facet polyhedron with a particle size of 5 μm, which are similar to the report of Bi [23]. The lattice-resolved HRTEM image of $PbMoO_4$ indicates that the lattice spacing is 0.324 nm, which is consistent with the (1 1 2) plane of wulfenite $PbMoO_4$. No obvious change in the lattice structure of $PbMoO_4$ is observed after C_{60} is modified, which is in accordance with the XRD analysis. However, after the introduction of C_{60}, defects are visible on the surface of $PbMoO_4$ (Fig. 2b), which can be attributed to the decreased crystallinity. During the hydrothermal process, C_{60} was adsorbed onto or bonded to the newly formed $PbMoO_4$ nucleus, which suppressed the growth of $PbMoO_4$, resulting in the crystal defects [43].

To investigate the C_{60} covering the surface of $PbMoO_4$, energy-dispersive spectrometry (EDS) was employed to analyze the element composition of C_{60}–$PbMoO_4$. As shown in Fig. 2c and d, there is a large amount of carbon on the surface of C_{60}–$PbMoO_4$, which can be attributed to the fact that the introduced C_{60} formed a layer coating the surface of $PbMoO_4$. Considering C_{60}–$PbMoO_4$ was washed with water and ethanol several times, C_{60} that physically adsorbed on the surface of $PbMoO_4$ can be washed away. Therefore, it can be concluded that a tight intact was formed between C_{60} layer and $PbMoO_4$.

The DRS spectra of the C_{60}–$PbMoO_4$ with different contents of C_{60} are shown in Fig. 3a. $PbMoO_4$ showed an absorption edge around 400 nm, corresponding to band-gap energy of about 3.1 eV. With the increase of the loading amount of C_{60} from 0.2 wt% to 5.0 wt%, the absorption wavelength range of the $PbMoO_4$ extended toward visible light. By plotting $(\alpha h\nu)^{1/2}$ versus $h\nu$, in which α being the absorption coefficient, the band-gap energies were calculated

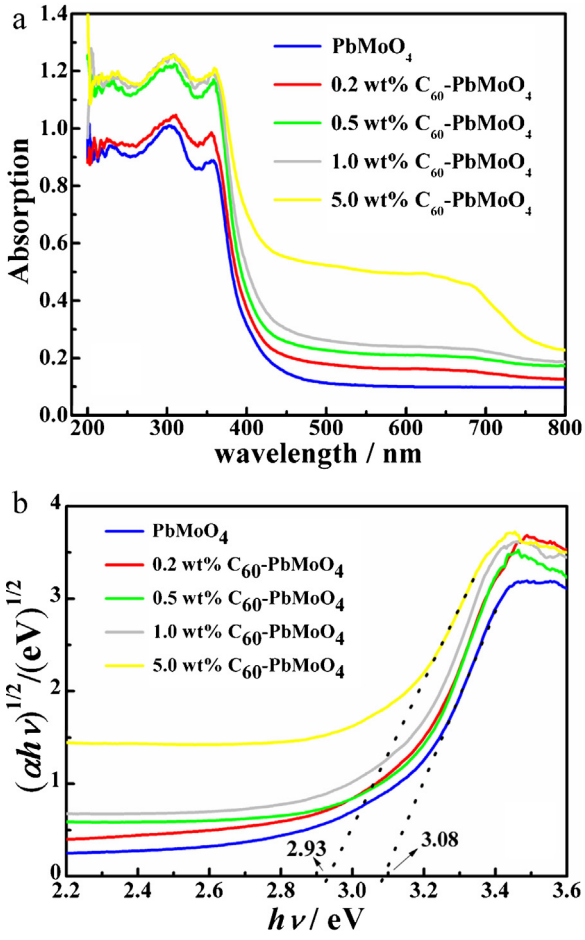

Fig. 3. (a) UV–vis diffuse reflection spectra of $PbMoO_4$ and C_{60}–$PbMoO_4$ with various contents of C_{60}. (b) Plot of $(\alpha h\nu)^{1/2}$ versus photon energy ($h\nu$) according to the DRS in (a).

(Fig. 3b) to be 3.08, 3.08, 3.07, 3.05, and 2.93 eV for $PbMoO_4$ and 0.2, 0.5, 1.0, and 5.0 wt% C_{60}–$PbMoO_4$, respectively. This shows that C_{60} can shift the absorption edge of $PbMoO_4$ to the visible light range and narrow the band-gap, which may be beneficial for improving the photocatalytic activity of $PbMoO_4$ under visible light irradiation [44].

The Raman spectra of C_{60}, $PbMoO_4$, and 0.5 wt% C_{60}–$PbMoO_4$ are shown in Fig. 4. The specific band at 1467.0 cm^{-1} is assigned

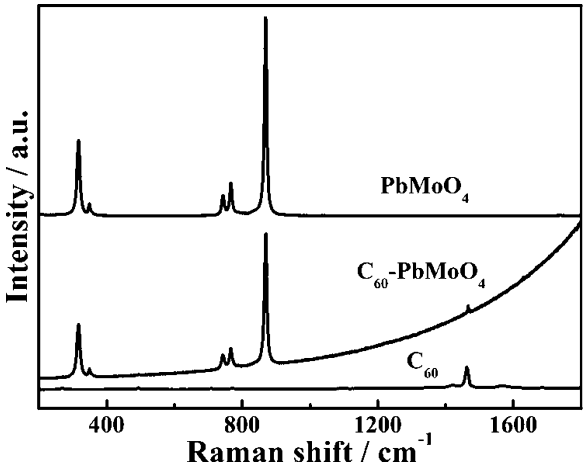

Fig. 4. Raman spectra of C_{60}, $PbMoO_4$, and C_{60}–$PbMoO_4$.

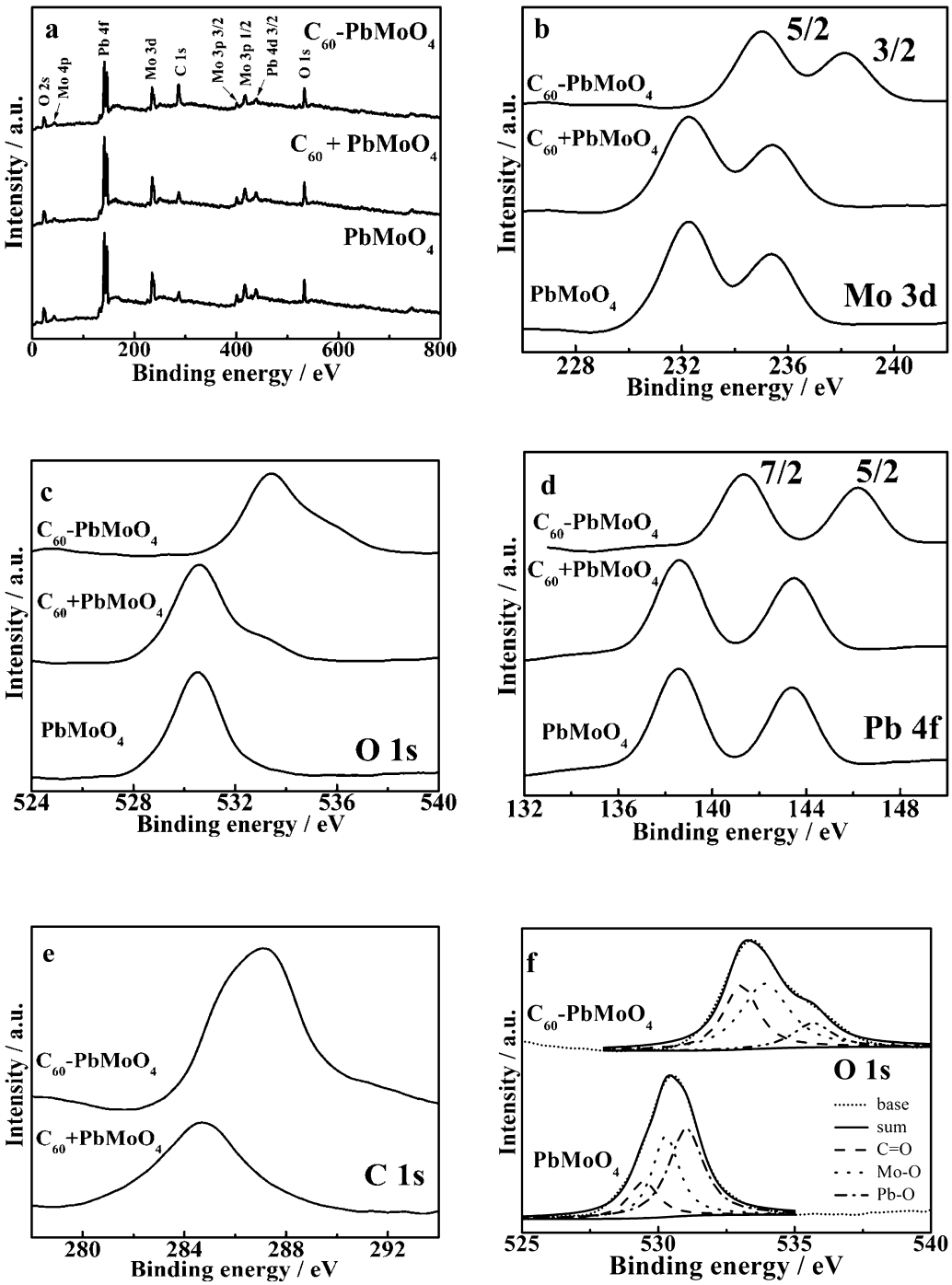

Fig. 5. XPS spectra: survey spectrum, Mo 3d, O 1s, Pb 4f, C 1s of $PbMoO_4$, C_{60} + $PbMoO_4$ and C_{60}–$PbMoO_4$.

to the bending vibration of C_{60} [45], and the characteristic band of $PbMoO_4$ is at 868.5 cm^{-1} [46]. Due to the small amount of C_{60} in C_{60}–$PbMoO_4$ and the good dispersion, the signal of C_{60} in C_{60}–$PbMoO_4$ is quite weak. However, the signal of C_{60} in C_{60}–$PbMoO_4$ suggests that C_{60} maintains its original structure after being bonded to the surface of $PbMoO_4$. According to the decrease of the characteristic band of C_{60}–$PbMoO_4$ at 868.5 cm^{-1}, it can be concluded that the crystallinity of $PbMoO_4$ was decreased due to the introduction of C_{60}, which is in accordance with the XRD results of C_{60}–$PbMoO_4$. These experimental results reveal that there maybe exist chemical interaction between C_{60} and $PbMoO_4$.

$PbMoO_4$, a mechanical mixture of functionalized C_{60} and $PbMoO_4$ (C_{60} + $PbMoO_4$), and C_{60}–$PbMoO_4$ were identified via XPS spectroscopy. XPS patterns of Mo 3d, O 1s, Pb 4f and C 1s for the $PbMoO_4$, C_{60} + $PbMoO_4$ and C_{60}–$PbMoO_4$ are shown in Fig. 5a [27,47,48]. As can be seen from Fig. 5b, the value of 232.3 eV for Mo 3d 5/2 can be assigned to a Mo^{6+} oxidation state in $PbMoO_4$. No obvious difference can be found between that of $PbMoO_4$ and C_{60} + $PbMoO_4$, but the binding energy of Mo 3d 5/2 increased from 232.3 eV in $PbMoO_4$ and C_{60} + $PbMoO_4$ to 235.0 eV in C_{60}–$PbMoO_4$. These experimental results indicates that mixing of C_{60} and $PbMoO_4$ would not change the chemical state of Mo, but the introduction of C_{60} via hydrothermal synthesis would change the chemical state of Mo. In addition, the binding energy of O 1s increased from 531.1 eV in $PbMoO_4$ and C_{60} + $PbMoO_4$ to 533.8 eV in C_{60}–$PbMoO_4$ (Fig. 5c), which indicates the change in the

chemical state of O. As discussed in our previous study on the carbon nanotube–TiO_2 hybrid [49,50], hydrothermal reaction would give birth to chemical bonding between carbon nanotube and TiO_2. In this study, the change in the chemical state of Mo also predicted some kind of chemical bonding was formed between C_{60} and $PbMoO_4$, which would inevitably affect the photocatalytic activity of C_{60}–$PbMoO_4$.

The binding energy of Pb 4f 5/2 in C_{60}–$PbMoO_4$ is 146.2 eV (Fig. 5d), which is 2.8 eV higher than that of pure $PbMoO_4$ (143.4 eV), represented the increasing of the electron density around the Pb^{2+} ions after modified by C_{60}. The binding energy of C 1s in C_{60}–$PbMoO_4$ increases to 287.1 eV, whereas it is 284.7 eV in the mechanical mixture of functionalized C_{60} and $PbMoO_4$ as well as in pure C_{60}. These phenomena indicate that the C_{60}–$PbMoO_4$ prepared via the hydrothermal process possesses a strong binding between C_{60} and $PbMoO_4$, whereas there is no strong binding in the C_{60} + $PbMoO_4$.

Signal deconvolution with a Gaussian curve fitting for O 1s in $PbMoO_4$ and C_{60}–$PbMoO_4$ is shown in Fig. 5f. The peaks in the curve for O 1s in $PbMoO_4$ were attributed to the bond of Mo–O at 530.3 eV, the bond of Pb—O at 531.1 eV, and the bond of C=O at the surface of $PbMoO_4$ at 529.5 eV, respectively. The increasing of the intensity of C=O and C 1s of C_{60}–$PbMoO_4$ indicated that the C=O bonds may have been formed between the C_{60} and $PbMoO_4$.

3.2. Photocatalytic activities

The photocatalytic activities of $PbMoO_4$, C_{60} + $PbMoO_4$ and C_{60}–$PbMoO_4$ were tested upon the degradation of RhB under UV light and visible light irradiation. As Fig. 6a shows, the photolysis test confirmed that RhB degraded rarely under UV light irradiation in the absence of photocatalyst. Only 37% RhB could be degraded over pure $PbMoO_4$ after UV light irradiation of 2 h. The photocatalytic activity of mechanical mixture of C_{60} and $PbMoO_4$ (C_{60} + $PbMoO_4$) was a little higher than that of pure $PbMoO_4$, which can be attributed to that C_{60} can arouse rapid photoinduced charge separation and reduce electron–hole recombination [51]. It should be underlined that all C_{60}–$PbMoO_4$ samples exhibited better photocatalytic activities than those of pure $PbMoO_4$ and C_{60} + $PbMoO_4$. With regard to the 0.5 wt% C_{60}–$PbMoO_4$ and 0.5 wt% C_{60} + $PbMoO_4$, the photocatalytic activity of former is almost as twice as that of latter.

The S_{BET} of $PbMoO_4$ and C_{60}–$PbMoO_4$ are measured to be 0.31 $m^2\ g^{-1}$ and 0.45 $m^2\ g^{-1}$, respectively. The S_{BET} of $PbMoO_4$ and C_{60}–$PbMoO_4$ is quite close, which indicates the difference in surface areas of $PbMoO_4$ and C_{60}–$PbMoO_4$ do not have a dominant effect on their photocatalytic activities. In addition, in our recent study [26], it was found that the photocatalytic activity of the $PbMoO_4$ microcrystals is more directly related to its surface structures or morphology rather than its specific surface area. The enhanced photocatalytic activity of C_{60}–$PbMoO_4$ could be explained by the fast transfer of photogenerated electrons and high charge separation efficiency in C_{60}–$PbMoO_4$, because C_{60} can act as "electron acceptors" [38,39,52] and the intimate contact (i.e. chemical bonding) between C_{60} and $PbMoO_4$ formed in the hydrothermal process is beneficial for the electron transfer.

In addition, the mass ratio of C_{60} has a great influence on the photocatalytic activity of the C_{60}–$PbMoO_4$ samples. After the introduction of 0.2 wt% C_{60}, the photocatalytic activity of $PbMoO_4$ can be increased largely. Among all photocatalysts containing $PbMoO_4$, 0.5 wt% C_{60}–$PbMoO_4$ showed the best photocatalytic activity, which is about 3.8 times higher than that of pure $PbMoO_4$. Further enhancing the proportion of C_{60} in C_{60}–$PbMoO_4$ led to a gradually decrease in the degradation rate of RhB though it remained higher than that of the bare $PbMoO_4$. The decrease in photoactivity at higher C_{60} mass ratio may be attributed to the fact that too much C_{60} in the composite would lead to a high recombination rate of photogenerated electrons and holes.

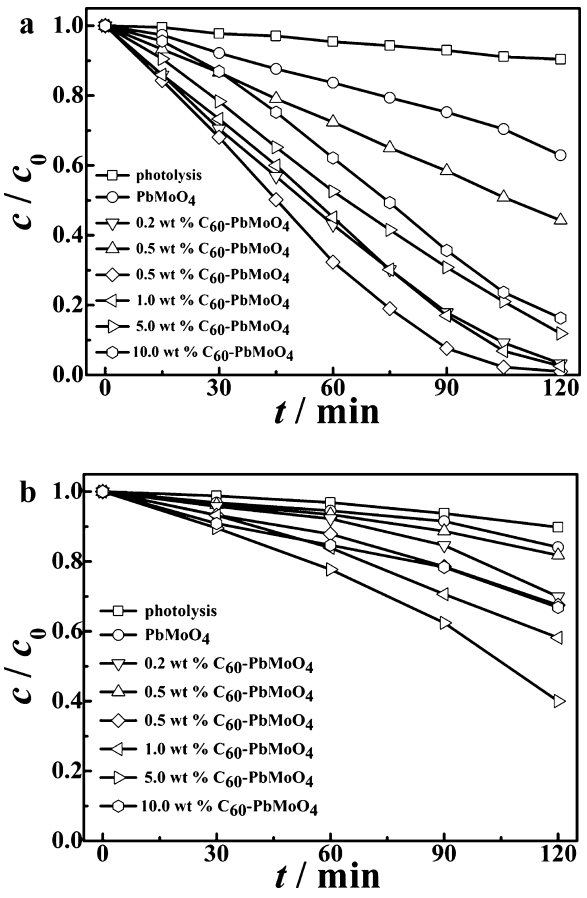

Fig. 6. Photocatalytic degradation of RhB over $PbMoO_4$ and C_{60}–$PbMoO_4$ under UV light irradiation (a) and visible light irradiation (b).

The photocatalytic activities of the samples under visible light irradiation were also investigated. As depicted in Fig. 6b, the degradation of RhB was negligible by the photolysis. Although the sensitization effect of RhB on its photocatalytic degradation can increase the degradation efficiency [53], RhB degraded rarely over pure $PbMoO_4$, which might imply the sensitization effect of RhB was weak upon pure $PbMoO_4$. As expected, C_{60} + $PbMoO_4$ demonstrated similar photoactivity to that of pure $PbMoO_4$. However, all samples of C_{60}–$PbMoO_4$ showed much higher photocatalytic activities than those of pure $PbMoO_4$ and C_{60} + $PbMoO_4$. The degradation rate of RhB over C_{60}–$PbMoO_4$ increased sustainedly with the mass ratio of C_{60} increasing from 0.2 wt% to 5.0 wt%, and then decreased with further increment. 5.0 wt% C_{60}–$PbMoO_4$ displayed the greatest photocatalytic activity, demonstrating an increase of about 4.1 times compared with that of pure $PbMoO_4$.

To test the stability of C_{60}–$PbMoO_4$, 0.5 wt% C_{60}–$PbMoO_4$ after photocatalytic reactions were collected and dried for the subsequent photocatalytic reaction cycles. Five cycles of the RhB removal experiments under an 18 W low-pressure mercury lamp were performed under the same experimental conditions and the result is shown in Fig. 7. The photoactivity of the photocatalyst used remains 92.6% after 5 recycles and did not exhibit any significant loss, implying that the as-prepared particles have a good photostability.

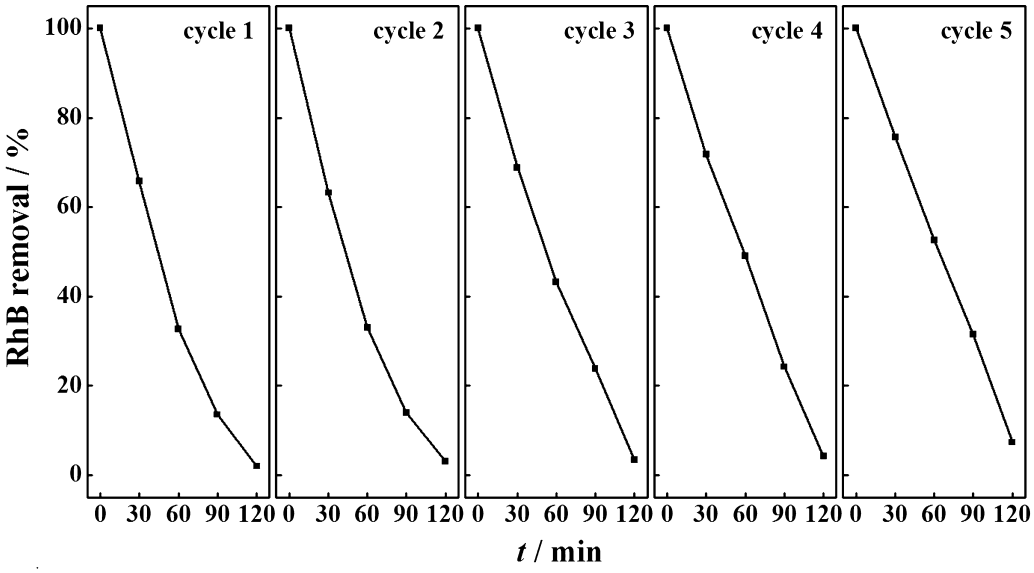

Fig. 7. Stability study of photocatalytic degradation of RhB over 0.5 wt% C_{60}–$PbMoO_4$ under UV light irradiation.

To uncover the effect of C_{60} modification on the stability of $PbMoO_4$, the remnant RhB solutions containing pure $PbMoO_4$ and C_{60}–$PbMoO_4$ after 10 h of UV light irradiation (five cycles) were detected through graphite furnace atomic absorbance spectrometry. In the RhB solution containing pure $PbMoO_4$, 98.3 $\mu g\,L^{-1}$ Pb^{2+} was found, which is about 0.0049% to the whole $PbMoO_4$ added into the suspension. However, after UV light irradiated for 10 h, there is only 0.75 $\mu g\,L^{-1}$ Pb^{2+} detected for the RhB solution containing C_{60}–$PbMoO_4$, which is about 0.00019% to the whole C_{60}–$PbMoO_4$ added. These experimental results indicate C_{60}–$PbMoO_4$ has a good photostability and chemical stability and C_{60} modification could largely increase the chemical stability of $PbMoO_4$.

3.3. Possible mechanism

As demonstrated by the experimental results, C_{60}–$PbMoO_4$ exhibits significant enhancement compared with pure $PbMoO_4$.

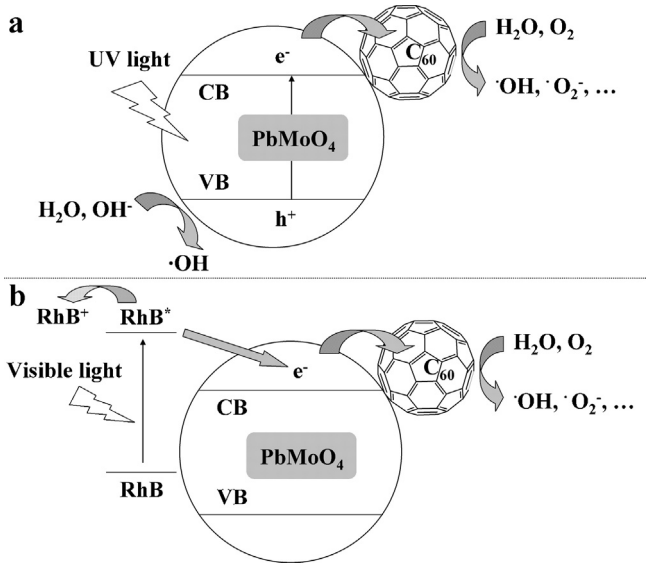

Fig. 8. The schematic of photocatalytic mechanism under UV light irradiation (a) and visible light irradiation (b).

Under UV light irradiation, the enhancement of photocatalytic activity can be attributed to the effective transfer of the photoinduced electrons from the conduction band of $PbMoO_4$ to C_{60} (Fig. 8a), which is facilitated by the delocalized π electrons of C_{60} [54].

Under visible light irradiation, the photocatalytic activity of C_{60}–$PbMoO_4$ is also largely enhanced compared with that of pure $PbMoO_4$. As illustrated in Fig. 8b, when the suspension containing RhB and C_{60}–$PbMoO_4$ is irradiated by visible light ($\lambda > 420$ nm), RhB can be stimulated to the excited state (RhB*), and the electrons of RhB* adsorbed on the surface of $PbMoO_4$ can be injected into the conduction band of the $PbMoO_4$ because of the suitable energy level between the conduction band of $PbMoO_4$ and the RhB*. Meanwhile, RhB* is converted into the cationic radical ($RhB^{\bullet+}$). In the absence of C_{60}, most of these electrons quickly recombine with $RhB^{\bullet+}$. However, in the case of C_{60}–$PbMoO_4$, the electrons can quickly transfer from the conduction band of the $PbMoO_4$ to C_{60} according to the conduction band position of $PbMoO_4$ and the potential of $C_{60}/C_{60}^{\bullet-}$. This transfer results in an efficient charge separation and a low recombination rate. Hence, a much higher photocatalytic activity under visible light irradiation can be obtained.

4. Conclusions

C_{60}–$PbMoO_4$ was synthesized via a hydrothermal method and employed in the photocatalytic degradation of RhB. The introduced C_{60} formed a layer coating the surface of $PbMoO_4$, which reduces the crystallite size of $PbMoO_4$ and increases the light absorption in the visible light region. Compared with a mixture of C_{60} and $PbMoO_4$ (C_{60} + $PbMoO_4$), the chemical states of Mo and Pb in C_{60}–$PbMoO_4$ are changed, indicating chemical bonding was formed between C_{60} and $PbMoO_4$ via hydrothermal reaction. In addition, C_{60}–$PbMoO_4$ showed better photocatalytic activities than those of pure $PbMoO_4$ and C_{60} + $PbMoO_4$, which indicates the interfacial contact between C_{60} and $PbMoO_4$ play important roles in the photocatalysis. The photocatalytic activity of $PbMoO_4$ increased 3.8 times at a C_{60} weight ratio of 0.5 wt% under UV light irradiation, and 4.1 times at a C_{60} weight ratio of 5.0 wt% under visible light irradiation. The enhanced photocatalytic activity of C_{60}–$PbMoO_4$ can be rationalized by the effective transfer of the photoinduced electrons on the interface of C_{60}

and $PbMoO_4$ and the strong light absorption in the visible light region.

Acknowledgments

The research was financially supported by the Doctoral Fund of Ministry of Education (20100146110004) of China and the Natural Science Foundation of Hubei Province (2011CDB139).

References

[1] A. Mittal, J. Mittal, A. Malviya, D. Kaur, V.K. Gupta, J. Colloid Interface Sci. 343 (2010) 463–473.
[2] V.K. Gupta, A. Rastogi, A. Nayak, J. Colloid Interface Sci. 342 (2010) 533–539.
[3] V.K. Gupta, I. Ali, V.K. Saini, Water Res. 41 (2007) 3307–3316.
[4] A.K. Jain, V.K. Gupta, A. Bhatnagar, Suhas, Sep. Sci. Technol. 38 (2003) 463–481.
[5] V.K. Gupta, A. Mittal, L. Kurup, J. Mittal, J. Colloid Interface Sci. 293 (2006) 16–26.
[6] V.K. Gupta, R. Jain, S. Varshney, J. Hazard. Mater. 142 (2007) 443–448.
[7] V.K. Gupta, A. Mittal, A. Malviya, J. Mittal, J. Colloid Interface Sci. 335 (2009) 24–33.
[8] V.K. Gupta, B. Gupta, A. Rastogi, S. Agarwal, A. Nayak, J. Hazard. Mater. 186 (2011) 891–901.
[9] V.K. Gupta, A. Mittal, L. Kurup, J. Mittal, J. Colloid Interface Sci. 304 (2006) 52–57.
[10] V.K. Gupta, R. Jain, S. Varshney, J. Colloid Interface Sci. 312 (2007) 292–296.
[11] R. Saravanan, V.K. Gupta, T. Prakash, V. Narayanan, A. Stephen, J. Mol. Liq. 178 (2013) 88–93.
[12] R. Saravanan, E. Thirumal, V.K. Gupta, V. Narayanan, A. Stephen, J. Mol. Liq. 177 (2013) 394–401.
[13] T.A. Saleh, V.K. Gupta, J. Colloid Interface Sci. 371 (2012) 101–106.
[14] V.K. Gupta, R. Jain, A. Mittal, T.A. Saleh, A. Nayak, S. Agarwal, S. Sikarwar, Mater. Sci. Eng. C 32 (2012) 12–17.
[15] V.K. Gupta, R. Jain, S. Agarwal, M. Shrivastava, Colloids Surf. A 378 (2011) 22–26.
[16] V.K. Gupta, R. Jain, S. Agarwal, A. Nayak, M. Shrivastava, J. Colloid Interface Sci. 366 (2012) 135–140.
[17] V.K. Gupta, R. Jain, A. Mittal, M. Mathur, S. Sikarwar, J. Colloid Interface Sci. 309 (2007) 464–469.
[18] R.M. Navarro Yerga, M.C. Álvarez-Galván, F. Del Valle, J.A. Villoria De La Mano, J.L.G. Fierro, ChemSusChem 2 (2009) 471–485.
[19] R. Saravanan, S. Karthikeyan, V.K. Gupta, G. Sekaran, V. Narayanan, A. Stephen, Mater. Sci. Eng. C 33 (2013) 91–98.
[20] W. Liu, M. Ji, S. Chen, J. Hazard. Mater. 186 (2011) 2001–2008.
[21] D. Li, Y. Zhu, CrystEngComm 14 (2012) 1128–1134.
[22] M. Zhang, C. Shao, J. Mu, X. Huang, Z. Zhang, Z. Guo, P. Zhang, Y. Liu, J. Mater. Chem. 22 (2012) 577–584.
[23] J. Bi, L. Wu, Y. Zhang, Z. Li, J. Li, X. Fu, Appl. Catal. B: Environ. 91 (2009) 135–143.
[24] Q. Chen, Q. Wu, Catal. Commun. 24 (2012) 85–89.
[25] M. Shen, Q. Zhang, H. Chen, T. Peng, CrystEngComm 13 (2011) 2785–2791.
[26] M. Shen, X. Zhang, K. Dai, H. Chen, T. Peng, CrystEngComm 15 (2013) 1146–1152.
[27] T. Zhou, J. Hu, J. Li, Appl. Catal. B: Environ. 110 (2011) 221–230.
[28] F. Duan, Y. Zheng, M. Chen, Mater. Lett. 65 (2011) 191–193.
[29] T.K. Ghorai, D. Dhak, S.K. Biswas, S. Dalai, P. Pramanik, J. Mol. Catal. A: Chem. 273 (2007) 224–229.
[30] F. Zhou, R. Shi, Y. Zhu, J. Mol. Catal. A: Chem. 340 (2011) 77–82.
[31] Y. Wang, J. Lin, R. Zong, J. He, Y. Zhu, J. Mol. Catal. A: Chem. 349 (2011) 13–19.
[32] T.A. Saleh, S. Agarwal, V.K. Gupta, Appl. Catal. B 106 (2011) 46–53.
[33] V.K. Gupta, S. Agarwal, T.A. Saleh, Water Res. 45 (2011) 2207–2212.
[34] Z. Shi, Y. Li, S. Wang, Z. Guo, C. Du, S. Xiao, N. Sun, Y. Cao, J. Yao, D. Zhu, E. Gao, S. Cai, Chem. Phys. Lett. 336 (2001) 19–23.
[35] L. Zhang, Y. Wang, T. Xu, S. Zhu, Y. Zhu, J. Mol. Catal. A: Chem. 331 (2010) 7–14.
[36] T. Hirakawa, P.V. Kamat, J. Am. Chem. Soc. 127 (2005) 3928–3934.
[37] X. Zhao, H. Liu, Y. Shen, J. Qu, Appl. Catal. B: Environ. 106 (2011) 63–68.
[38] H. Fu, T. Xu, S. Zhu, Y. Zhu, Environ. Sci. Technol. 42 (2008) 8064–8069.
[39] S. Zhu, T. Xu, H. Fu, J. Zhao, Y. Zhu, Environ. Sci. Technol. 41 (2007) 6234–6239.
[40] K. Dai, T. Peng, D. Ke, B. Wei, Nanotechnology 20 (2009) 125603.
[41] J. Li, S.K. Cushing, J. Bright, F. Meng, T.R. Senty, P. Zheng, A.D. Bristow, N. Wu, ACS Catal. 3 (2013) 47–51.
[42] S.K. Cushing, J. Li, F. Meng, T.R. Senty, S. Suri, M. Zhi, M. Li, A.D. Bristow, N. Wu, J. Am. Chem. Soc. 134 (2012) 15033–15041.
[43] D. Kim, K.D. Min, J. Lee, J.H. Park, J.H. Chun, Mater. Sci. Eng. B 131 (2006) 13–17.
[44] Y. Long, Y. Lu, Y. Huang, Y. Peng, Y.J. Lu, S.Z. Kang, J. Mu, J. Phys. Chem. C 113 (2009) 13899–13905.
[45] G.G. Siu, Y. Liu, S. Xie, J. Xu, T. Li, L. Xu, Thin Solid Films 274 (1996) 147–149.
[46] A. Phuruangrat, T. Thongtem, S. Thongtem, J. Cryst. Growth 311 (2009) 4076–4081.
[47] A.A. Arie, J.K. Lee, J. Nanosci. Nanotechnol. 12 (2012) 1658–1661.
[48] R. Iordanova, M. Mancheva, Y. Dimitriev, D. Klissurski, G. Tyuliev, B. Kunev, J. Alloys Compd. 485 (2009) 104–109.
[49] K. Dai, X. Zhang, K. Fan, T. Peng, B. Wei, Appl. Surf. Sci. 270 (2013) 238–244.
[50] C. Liu, H. Chen, K. Dai, A. Xue, H. Chen, Q. Huang, Mater. Res. Bull. 48 (2013) 1499–1505.
[51] S.K. Hong, J.H. Lee, W.B. Ko, J. Nanosci. Nanotechnol. 11 (2011) 6049–6056.
[52] J. Yu, T. Ma, G. Liu, B. Cheng, Dalton Trans. 40 (2011) 6635–6644.
[53] J. Shang, F. Zhao, T. Zhu, J. Li, Sci. China Ser. B 54 (2011) 167–172.
[54] T. Hasobe, H. Imahori, S. Fukuzumi, P.V. Kamat, J. Phys. Chem. B 107 (2003) 12105–12112.